Available online at www.sciencedirect.com
SCIENCE DIRECT
Journal of Solid State Chemistry 179 (2006) 1668–1673
JOURNAL OF SOLID STATE CHEMISTRY
www.elsevier.com/locate/jssc

Synthesis, structure and physical properties of layered semiconductors MCuFCh (M = Sr, Eu, Ch = S, Se)

Eiji Motomitsu[a,b], Hiroshi Yanagi[a], Toshio Kamiya[a,b], Masahiro Hirano[b], Hideo Hosono[a,b,c,*]

[a] *Materials and Structures Laboratory, Tokyo Institute of Technology, 4259, Nagatsuta, Midori-ku, Yokohama 226-8503, Japan*
[b] *ERATO-SORST, Japan Science and Technology Agency (JST), Frontier Collaborative Research Center, Tokyo Institute of Technology, 4259 Nagatsuta, Midori-ku, Yokohama 226-8503, Japan*
[c] *Frontier Collaborative Research Center, Tokyo Institute of Technology, 4259 Nagatsuta, Midori-ku, Yokohama 226-8503, Japan*

Received 11 November 2005; received in revised form 20 February 2006; accepted 26 February 2006

Abstract

Effects of open shell cations on magnetic, optical and carrier transport properties were examined for layered wide bandgap semiconductors MCuFCh (M = Sr, Eu, Ch = S, Se). Single-phase MCuFCh powder and ceramic samples were synthesized by solid-state reactions. The crystal structures refined by the Rietveld analyzes revealed that all the materials have the space group $P4/nmm$, indicating that the samples have the same crystal structure as that of layered oxychalcogenides LaCuOCh, and cation vacancies of several percent were present for Cu^+ and Eu^{2+} sites in EuCuFCh. Thermopower measurements revealed that both SrCuFCh and EuCuFCh were p-type semiconductors. Degenerate conduction was observed for EuCuFCh with conductivities $>1\,S\,cm^{-1}$, whereas SrCuFCh exhibited thermally activated behavior. The optical band gaps of SrCuFS and SrCuFSe estimated were approximately 3.0 and 2.7 eV, respectively, and those of EuCuFCh were ~2 eV. Temperature dependence of magnetic susceptibilities of EuCuFCh followed the Curie–Weiss law down to 5 K and the samples did not show any transition to a magnetic ordering phase.

Keywords: Layered structure; Fluoridechalcogenide; Wide-gap semiconductor

1. Introduction

Magnetic semiconductors and diluted magnetic semiconductors (DMSs) show interesting properties due to exchange interactions between magnetic moments on ions and spins of charge carriers. As for DMS, the discovery of ferromagnetism in Mn-doped GaAs has attracted researchers to this field: however, the magnetic transition temperature is still as low as ~170 K [1]. For practical applications, intensive effort has been carried out to realize room-temperature ferromagnetism by, e.g. improving deposition technique and/or exploring a new host material. Dietl et al. suggested theoretically that room-temperature ferromagnetism would be attained in a material which satisfies: (1) p-type conduction, (2) carrier concentration greater than $10^{20}\,cm^{-3}$, and (3) wide band gap [2]. It triggered fever of the DMS researches using transparent conducting oxides (TCOs) as host materials [3–5], because TCOs have a wide band gap of >3 eV and carrier concentration may be controlled from $<10^{16}$ to $\sim10^{21}\,cm^{-3}$, even though almost all the TCOs are not p-type but n-type conductors.

For the last decade, we have explored new p-type TCOs and wide band gap oxychalcogenides based on our original strategy [6]. In the discovered p-type materials, LaCuOCh (Ch = S, Se) has interesting properties. Hole concentration can run up to $>10^{20}\,cm^{-3}$ and degenerate conduction may be attained, which have not yet been achieved in other p-type wide bandgap semiconductors including GaN. They exhibit sharp absorption peaks and photoluminescence peaks near the absorption edge, which originates from room-temperature stable excitons [6,7]. One of the origins

*Corresponding author. Frontier Collaborative Research Center, Tokyo Institute of Technology, 4259 Nagatsuta, Midori-ku, Yokohama 226-8503, Japan. Fax: +81 45 924 5339.
E-mail address: hosono@msl.titech.ac.jp (H. Hosono).

0022-4596/$ - see front matter © 2006 Elsevier Inc. All rights reserved.
doi:10.1016/j.jssc.2006.02.031

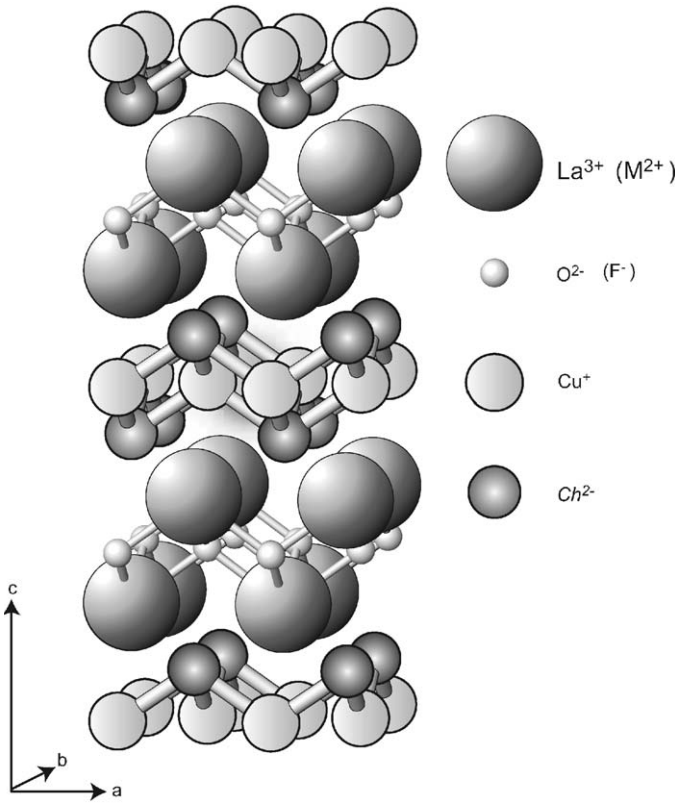

Fig. 1. Crystal structure of LaCuO*Ch* (*Ch* = S, Se). La^{3+} and O^{2-} are replaced with M^{2+} and F^{-}, respectively, for *M*CuF*Ch* (*M* = Eu, Sr).

of these properties comes from its crystal structure (Fig. 1). It has a layered structure with a tetragonal symmetry in which hole conduction paths formed of $(Cu_2Ch_2)^{2-}$ layers are sandwiched between wider gap $(La_2O_2)^{2+}$ layers. This 2-D electronic structure is thought to lead to high hole mobility and thermal stability of excitons [8].

We have reported optical and electrical properties of *Ln*CuO*Ch* [9,10], in which La in LaCuO*Ch* is replaced with trivalent lanthanide cations (*Ln* = Ce^{3+}, Pr^{3+}, Nd^{3+}), to examine possibility of band engineering and of alternation of optoelectronic properties. Eu^{2+} compounds are of another interest because it was expected to exhibit magnetic functions due to the large spin moment of a Eu^{2+} ion (note that Eu^{3+} compounds usually have small magnetic polarization). For example, EuO and EuS are well-known ferromagnetic semiconductors. An approach to substitute a divalent cation for the trivalent lanthanide cations by keeping the same layered crystal structure is to substitute a monovalent anion for the divalent chalcogen anions simultaneously. Recently an example was reported as BaCuF*Ch*, whose crystal structure is the same as LaCuO*Ch* though the trivalent cation (La^{3+}) is replaced with the divalent cation (Ba^{2+}) [11]. The oxide layers in *Ln*CuO*Ch* are simply replaced with the fluoride layers in BaCuF*Ch*, and hole conduction paths are still in the $(Cu_2Ch_2)^{2-}$ layers, keeping the fascinating features of *Ln*CuO*Ch*. In fact, BaCuF*Ch* shows p-type degenerated conduction even without intentional impurity doping [12,13].

In the present study, we prepared *M*CuF*Ch* (*M* = Eu, Sr, *Ch* = S, Se) by solid-state reaction. Sr^{2+} was selected as a non-magnetic ion for reference to EuCuF*Ch* as its ion radius is almost the same as that of Eu^{2+} [14]. SrCuF*Ch* was briefly reported [15] but details of crystal structure and physical properties have not been examined. Existence of trace impurity phases was carefully examined using a high-power rotary Cu target tube X-ray diffraction (XRD) apparatus. The crystal structures of *M*CuF*Ch* were examined by the Rietveld analyzes. Electrical, optical and magnetic properties were measured using the single-phase samples.

2. Experiments

*M*CuF*Ch* were synthesized by solid-state reaction of MF_2, *MCh*, and Cu_2Ch. As the chemicals used are air and moisture sensitive, all the mixing procedures were carried out in a glove box in dry Ar gas at −70 °C dewpoint. First, we prepared starting materials. EuF_2 powder was prepared by reduction of EuF_3 in a flowing H_2 gas at 1000 °C for 10 h. SrS powder was prepared by reduction of $SrSO_4$ in a flowing H_2 gas at 1100 °C for 15 h. SrSe and EuSe powders were prepared by reactions of Se with Sr at 450 °C and with Eu metal at 700 °C for 5 h in evacuated silica tubes. The stoichiometric mixtures of the starting materials were pressed into pellets and again sealed in evacuated silica tubes, followed by heating at 500 °C for 6 h and at 750 °C for 6 h for SrCuF*Ch* and EuCuF*Ch*, respectively. Powder XRD patterns of the obtained samples were measured by a diffractometer (RINT-2500, Rigaku) equipped with a rotary Cu target and a monochrometer to separate $K\alpha_1$ and $K\alpha_2$ radiation. The XRD data were collected from $2\theta = 5^\circ$ to 140° with a scan step of 0.01°. The sampling time was 4 s for each sampling angle. The crystal structures were refined by the Rietveld method using the program code, RIETAN-2000 [16]. The space group of *P*4/*nmm* was employed, and initial parameters for the iterative refinement procedure were taken from the crystal structure data of BaCuFSe [11].

DC electrical conductivity was measured by a four-probe method (using PPMS, Quantum Design) using rectangular-solid-shaped sintered polycrystalline samples with sputtered parallel plate Au electrodes in the temperature range from 2 to 400 K. Seebeck coefficients were measured at room temperature to determine carrier polarity. Diffuse reflectance spectra of the powder samples were measured in the UV-visible region using a spectrophotometer (U-4000, Hitachi) at room temperature. The diffuse reflectance spectra were transformed to absorption spectra using the Kubelka–Munk equation to estimate optical band gaps [17]. Temperature dependences of DC magnetic susceptibility were measured for EuCuF*Ch* using powder samples with a SQUID magnetometer (MPMS, Quantum Design) in the temperature range from 5 to 300 K.

3. Results and discussion

Fig. 2 shows the XRD pattern of EuCuFS with the Rietveld analysis result as an example. Similar results were obtained on the other *M*CuF*Ch* compounds. The refined patterns agreed well with the measured XRD patterns, and no extra peak was observed, indicating single-phase samples were synthesized. The color of the single-phase powder SrCuFS was light yellow, and that of SrCuFSe was light brown. On the other hand, both the EuCuF*Ch* powders were dark green.

The lattice parameters, a and c, refined by the Rietveld analyzes, are summarized in Table 1 along with the unit cell volumes (V_{cell}) and reliability factors (R). Table 2 lists atomic positions, site occupation factors (occupancy) and isotropic thermal parameters (B). The difference in the lattice parameters between SrCuF*Ch* and EuCuF*Ch* are as small as 0.25%, which would be reasonable because the ionic radii of Sr^{2+} and Eu^{2+} are similar [14]. The interatomic distances were calculated from the refined crystal structures (denoted 'Obs' in Table 3) and as a sum of the ionic radii of neighboring ions ('Cal'), respectively. The ionic radii for eight-fold coordinated M^{2+} ions were taken from the Shannon's table of effective ion radii [14]. The observed *M*–F distances are ~4% shorter than the calculated values in all *M*CuF*Ch*. The observed *M*–*Ch* distances are ~2% longer than the calculated values in SrCuF*Ch*, while the differences are within only ±1% in EuCuF*Ch*.

Fig. 3 shows temperature dependence of electrical conductivities of *M*CuF*Ch* measured using the sintered polycrystalline samples. Room-temperature electrical conductivities of SrCuF*Ch* were as low as 8.4×10^{-5} S/cm for *Ch* = S and 3.6×10^{-3} S/cm for Se, and showed thermally activated behavior. The Seebeck coefficients of SrCuFS and SrCuFSe were +620 and +310 μV/K, respectively, indicating they are p-type semiconductors. On the other hand, the temperature dependences of EuCuF*Ch* showed degenerated and metallic conduction behavior. The conductivities at room temperature reached 1.9 S/cm for EuCuFS and 1.5×10^{1} S/cm for EuCuFSe. The Seebeck coefficients were positive (+14 μV/K for EuCuFS and +10 μV/K for EuCuFSe). These results confirmed that EuCuF*Ch* were also p-type semiconductors. The electrical properties are summarized in Table 4 with relative densities of the sintered polycrystalline samples and optical band gaps. Note that no intentional doping was carried out for all the samples here. Therefore, the holes in the *M*CuF*Ch* samples are presumed to generate through the formation of ionized cation vacancies and/or interstitial anions.

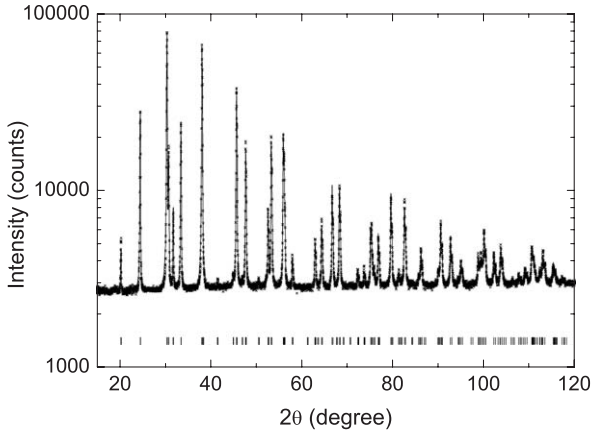

Fig. 2. XRD pattern of EuCuFS measured (×) and refined by RIETAN-2000 (solid line). The positions of the Bragg reflections are indicated in the bottom row by the vertical bars.

Table 1
Lattice parameters and reliability factors obtained by the crystal structure refinements for *M*CuF*Ch* (*M* = Eu, Sr, *Ch* = S, Se)

Formula	SrCuFS	EuCuFS	SrCuFSe	EuCuFSe
a (Å)	3.956(2)	3.949(2)	4.063(2)	4.057(2)
c (Å)	8.659(5)	8.642(3)	8.842(1)	8.815(2)
V_{cell} (Å^3)	135.5(1)	134.7(4)	146.0(1)	145.1(3)
R_p (%)	3.51	3.43	3.63	3.52
R_{wp} (%)	4.74	4.41	4.72	4.76
R_F (%)	1.81	1.67	1.73	1.82
R_e (%)	2.58	3.74	2.88	2.58

The values in parentheses show errors in the last digit.

Table 2
Site occupancy, fractional coordinates (x, y, z), and isotropic thermal parameters (B) of *M*CuF*Ch* (*M* = Eu, Sr, *Ch* = S, Se)

	WN	Occupancy	x	y	z	B (Å^2)
SrCuFS						
Sr	2*c*	1.0*	1/4	1/4	0.1677(1)	0.09(5)
Cu	2*b*	0.97(1)	1/4	3/4	0	0.85(5)
S	2*c*	1.0*	1/4	1/4	0.6648(3)	0.14(7)
F	2*a*	1.0*	1/4	3/4	$\frac{1}{2}$	0.50
EuCuFS						
Eu	2*c*	0.97(2)	1/4	1/4	0.1708(3)	0.64(4)
Cu	2*b*	0.94(1)	1/4	3/4	0	0.72(4)
S	2*c*	1.0*	1/4	1/4	0.6646(1)	0.54(2)
F	2*a*	0.98(1)	1/4	3/4	$\frac{1}{2}$	0.41(2)
SrCuFSe						
Sr	2*c*	0.98(3)	1/4	1/4	0.1601(2)	0.61(3)
Cu	2*b*	0.97(2)	1/4	3/4	0	0.76(4)
Se	2*c*	1.0*	1/4	1/4	0.6708(3)	0.62(1)
F	2*a*	1.0*	1/4	3/4	$\frac{1}{2}$	0.73(1)
EuCuFSe						
Eu	2*c*	0.98(2)	1/4	1/4	0.1635(3)	0.21(4)
Cu	2*b*	0.97(1)	1/4	3/4	0	0.65(2)
Se	2*c*	1.0*	1/4	1/4	0.6698(2)	0.61(4)
F	2*a*	1.0*	1/4	3/4	$\frac{1}{2}$	0.69(2)

The values in parentheses show errors in the last digit. The site occupancy values indicated with * were refined to be 1.00 or 1.01 with the errors of 0.01. The errors for occupancy and B would be underestimated because each of these parameters were refined independently and the other structural parameters (x, y, z) were fixed to avoid divergence of the refinement results.

Table 3
Interatomic distances in *M*CuF*Ch* (*M* = Eu, Sr, *Ch* = S, Se) calculated from the crystal refinement data (Obs) and estimated as the simple sum of the ionic radii (Cal)

Sample	*M*–F (Å)			*M*–*Ch* (Å)			Cu–*Ch* (Å)		
	Obs.	Cal.	Diff (%)	Obs.	Cal.	Diff (%)	Obs.	Cal.	Diff (%)
SrCuFS	2.472	2.57	−4.0	3.165	3.10	2.1	2.458	2.44	0.7
EuCuFS	2.471	2.56	−3.6	3.130	3.09	1.3	2.434	2.44	−0.3
SrCuFSe	2.476	2.57	−3.8	3.239	3.24	0.0	2.531	2.58	−1.9
EuCuFSe	2.489	2.56	−2.9	3.223	3.23	−0.2	2.521	2.58	−2.3
	La–O (Å)			La–*Ch* (Å)			Cu–*Ch* (Å)		
LaCuOS	2.362	2.56	−8.4	3.257	3.00	7.9	2.428	2.44	−0.5

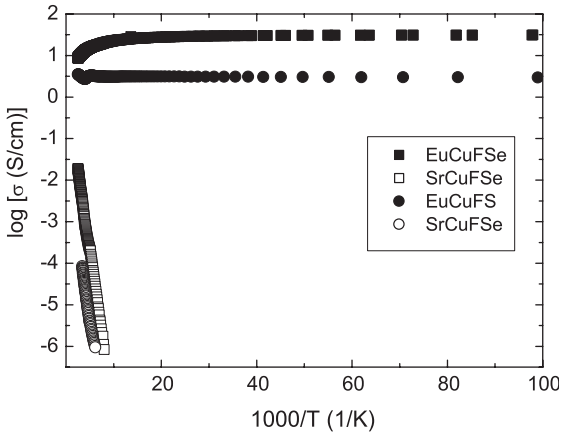

Fig. 3. Temperature dependences of electrical conductivity of *M*CuF*Ch* (*M* = Eu, Sr, *Ch* = S, Se).

Occupancies and thermal vibration factors are also refined by the Rietveld analyzes, and they are listed in Table 2. Note that in general it is difficult to obtain reliable parameters for occupancy and thermal vibration parameters using powder diffraction data. Here we took good signal-noise ratio data using the high-power XRD apparatus and examined the validity of the refinement results using different initial parameters and different refinement paths. Consistent and reasonable results were obtained by alternately refining the occupancies and thermal vibration parameters with fixed atomic positions (x, y, z). It is seen that the occupancies of Sr and *Ch* were all unity within errors of 1%. While, those of Eu and Cu show non-negligible deviation from unity systematically. Although the deviations are still small to make definitive discussion (i.e. smaller than 3σ of the standard deviation errors except for the Cu occupancy in EuCuFS), these results appear to be consistent with the electrical conductivities of *M*CuF*Ch* and give a plausible origin of the p-type conduction in *M*CuF*Ch*. It is thought that cation vacancies yield holes in ionic compounds, and the occupancy analyzes suggest that high-density Eu and Cu vacancies would be formed. Similar to LaCuO*Ch*, it would be plausible that p-type conduction in *M*CuF*Ch* is primarily attributed to the formation of Cu vacancies. In EuCuF*Ch*, Eu vacancy would also contribute to the hole generation, which gives the conductivities larger than SrCuF*Ch* and degenerate conduction. It would be useful to compare these results with those of a similar layered oxychalcogenide $La_2CdO_2Se_2$ [21]. No detectable deviation of occupancies from unity was observed for all the constituent atoms, and actually $La_2CdO_2Se_2$ did not show detectable electrical conductivity.

The absorption spectra derived from the Kubelka–Munk equation are shown in Fig. 4. In the cases of SrCuF*Ch* and EuCuFS, the clear band edge structures were observed, and the band gaps were estimated to be 3.1 eV for SrCuFS and 2.9 eV for SrCuFSe. The selenide has the smaller band gap than the sulfide has. This result is explained by the larger dispersion of the valence band top in the selenide than in the sulfide, similar to the LaCuO*Ch* system [7,19]. The band gap of EuCuFS was estimated to be 2.5 eV. By contrast, EuCuFSe spectra did not show clear band edge structure (a value >2 eV might be estimated if the very gentle slope in ~2–3 eV is assumed to be an absorption edge structure). It is speculated that the strong absorption around the absorption edge is probably associated with the high concentration vacancies, which might be supported by correlation between the sharpness of the absorption edge and the electrical conductivity.

Fig. 5 shows the temperature dependence of DC magnetic molar susceptibilities (χ_m) of EuCuF*Ch* measured using the powder samples. Both the samples followed the Curie–Weiss law and did not show a magnetic transition in the measured temperature range. The effective magnetic moments (μ_{eff}) evaluated from the Curie constants are 7.69 μ_B for EuCuFS and 7.42 μ_B for EuCuFSe (μ_B: Bohr magneton). These values are close to that of free europium divalent ion ($\mu_{eff} = 7.94\,\mu_B$), indicating that almost all the europium ions are divalent in the detection limit of the present measurements. The differences between measured and free ion's μ_{eff} are thought to come from the covalency and crystal field [18,20].

EuCuF*Ch* did not show any magnetic ordering though EuO and EuS are ferromagnetic semiconductors. This result can partly be explained by a theoretical calculation based on the FLAPW/LDA + U method and RPA approximation reported by Kuneš and Pickett [22]. They

Table 4
Electrical and optical properties of *M*CuF*Ch*

Sample	EuCuF*Ch*		SrCuF*Ch*	
Ch	S	Se	S	Se
Density (%)	84	81	89	87
Conductivity at RT (S/cm)	1.9	15	8.4×10^{-5}	3.6×10^{-3}
Seebeck coef. (μV/K)	+14	+10	+620	+310
Optical gap (eV)	2.5	(~2.0)	3.1	2.9
Color	Dark green	Dark green	Light yellow	Light brown

The optical gap value in parentheses for EuCuFSe is shown just for reference because it was speculated from the gentle slope in the ~2–3 eV range in Fig. 4 and not reliable.

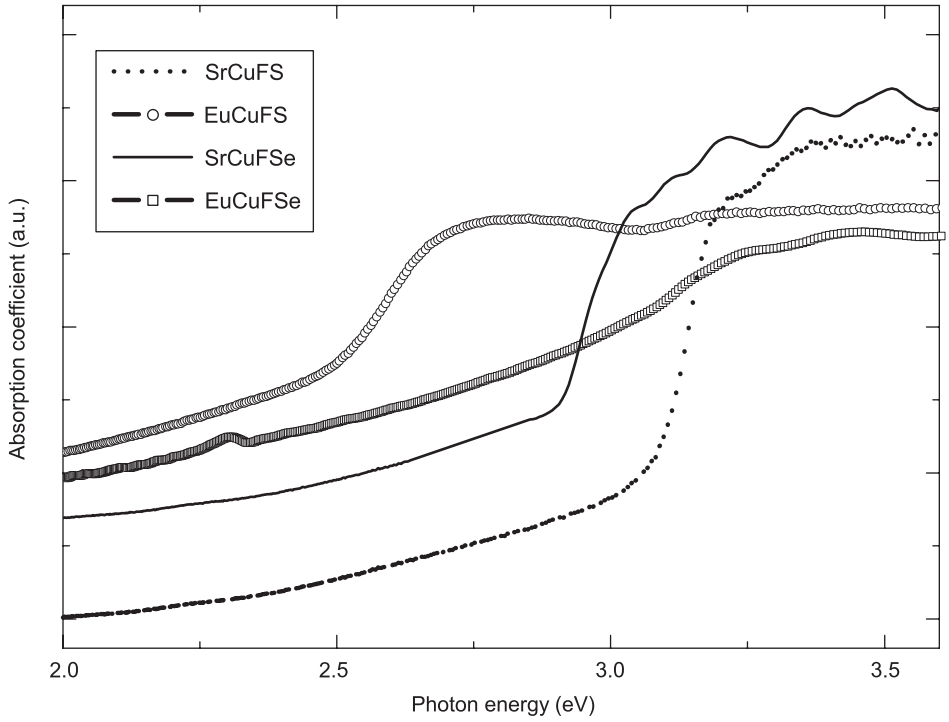

Fig. 4. Optical absorption spectra of *M*CuF*Ch* (*M* = Eu, Sr, *Ch* = S, Se) powder samples converted using the Kubelka–Munk equation from diffuse reflectance spectra.

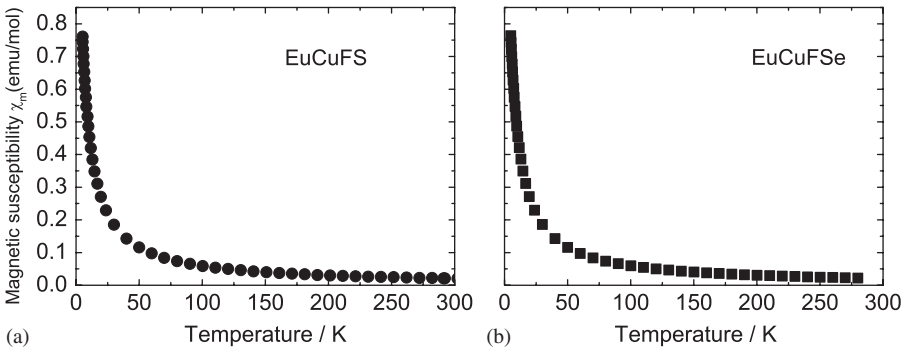

Fig. 5. Temperature dependences of magnetic susceptibility of: (a) EuCuFS and (b) EuCuFSe.

report that magnetic ordering temperature in rocksalt Eu*Ch* decreases with increasing the lattice constant (i.e. Eu–*Ch* distance). As seen in our Table 3, the Eu–*Ch* distances were 3.13 Å for EuCuFS and 3.22 Å for EuCuFSe (cf. Eu–*Ch* distances are 2.99 Å for EuS (ICSD# 53439) and 3.13 Å for EuSe (ICSD# 27109)). Their calculation

predicts that the ordering temperature becomes $\leqslant 0$ K at the Eu–*Ch* distance of ~3.09 Å. Therefore, the reason why a magnetic ordering state was not observed in EuCuF*Ch* can be attributed to the large Eu–*Ch* distances. Even though, we expected that generation of holes might assist to realize ferromagnetic states as believed in DMS, but it did not occur in EuCuF*Ch*. A possible explanation would be as follows. As an analog to LaCuO*Ch*, it is thought that carrier holes in EuCuF*Ch* run through the valence band maximum states, which is mainly composed of Cu 3*d* and *Ch np* ($n = 3$ for S and 4 for Se) orbitals. In addition, we measured ultraviolet photoelectron emission spectra and found that the Eu 4*f* levels were located at >2 eV below the valence band maximum (to be reported elsewhere). In this case, the exchange interaction between the mobile holes and the Eu 4*f* electrons is not strong enough to realize a magnetic ordering phase. In other words, (Cu 3*p*, *Ch np*)–Eu 4*f* interaction is weak due to the confined nature of Eu 4*f* orbitals and the layered structure of EuCuF*Ch*.

4. Conclusion

Single-phase samples of new materials *M*CuF*Ch* ($M =$ Eu, Sr, $Ch =$ S, Se) were synthesized by solid-state reactions. Their crystal structures were refined by the Rietveld method and discussed in relation to electrical and magnetic properties. *M*CuF*Ch* have the same layered structures as those of *Ln*CuO*Ch*, though $(Ln_2O_2)^{2+}$ layers are replaced with $(M_2F_2)^{2+}$ layers. All the obtained samples showed p-type conduction. Temperature dependences of conductivity of SrCuF*Ch* showed thermally activated behavior, while those of EuCuF*Ch* showed degenerated and metallic conduction. EuCuF*Ch* did not exhibit magnetic ordering transition in the temperature range from 5 to 300 K.

References

[1] A.M. Nuzmul, S. Sugahara, M. Tanaka, Phys. Rev. B 67 (2003) 241308.
[2] T. Dietl, H. Ohno, F. Matsukura, J. Cibert, D. Ferraned, Science 287 (2000) 1019.
[3] S. Sonoda, S. Shimizu, T. Sasaki, T. Yamamoto, H. Hori, J. Cryst. Growth 237 (2002) 1358.
[4] Y. Matsumoto, M. Murakami, T. Shono, T. Hasegawa, T. Fukumura, M. Kawasaki, A. Ahmet, T. Chikyow, S. Koshihara, H. Koinuma, Science 291 (2001) 854.
[5] K. Ueda, H. Tabata, T. Kawai, Appl. Phys. Lett. 79 (2001) 988.
[6] K. Ueda, S. Inoue, N. Sarukura, M. Hirano, H. Hosono, Appl. Phys. Lett. 78 (2001) 2333.
[7] H. Hiramatsu, K. Ueda, K. Takafuji, H. Ohta, M. Hirano, T. Kamiya, H. Hosono, J. Appl. Phys. 94 (2003) 5805.
[8] K. Ueda, H. Hiramatsu, H. Ohta, M. Hirano, T. Kamiya, H. Hosono, Phys. Rev. B 69 (2004) 155305.
[9] K. Ueda, K. Takafuji, H. Hiramatsu, H. Ohta, T. Kamiya, M. Hirano, H. Hosono, Chem. Mater. 15 (2003) 3692.
[10] K. Ueda, K. Takafuji, H. Hosono, J. Solid State Chem. 170 (2003) 182.
[11] W.J. Zhu, Y.Z. Huang, F. Wu, C. Dong, H. Chen, Z.X. Zhao, Mater. Res. Bull. 29 (1994) 505.
[12] H. Yanagi, J. Tate, S. Park, C. Park, D.A. Keszer, Appl. Phys. Lett. 82 (2003) 2814.
[13] H. Yanagi, S. Park, C. Park, A.D. Draeseke, D.A. Keszler, J. Tate, J. Solid State Chem. 103 (2003) 34.
[14] R.D. Shannon, Acta Crystallogr. A 32 (1976) 751.
[15] C.-H. Park, D.A. Keszler, H. Yanagi, J. Tate, Thin Solid Films 445 (2003) 288.
[16] F. Izumi, T. Ikeda, Mater. Sci. Forum 198 (2000) 321.
[17] P. Kubelka, F. Munk, Z. Tech. Phys. (Leipzig) 12 (1931) 593.
[18] K. Ueda, K. Takafuji, H. Hosono, J. Solid State Chem. 170 (2003) 182.
[19] K. Ueda, H. Hosono, J. Appl. Phys. 91 (2002) 4768.
[20] D.A. Maclean, K. Seto, J.E. Greedan, J. Solid State Chem. 40 (1981) 241.
[21] H. Hiramatsu, K. Ueda, T. Kamiya, H. Ohta, M. Hirano, H. Hosono, J. Mater. Chem. 14 (2004) 2946.
[22] J. Kuneš, W.E. Pickett, Physica B 359 (2005) 205.